HOKKAIDO UNIVERSITY

Title	Time Domain Wake Field Computation With Boundary Element Method
Author(s)	Fujita, Kazuhiro; Kawaguchi, Hideki; Zagorodnov, Igor et al.
Description	(c) 2006 IEEE. Personal use of this material is permitted. However, permission to reprint/republish this material for advertising or promotional purposes or for creating new collective works for resale or redistribution to servers or lists, or to reuse any copyrighted component of this work in other works must be obtained from the IEEE.
Citation	IEEE TRANSACTIONS ON NUCLEAR SCIENCE, 53(2), 431-439 https://doi.org/10.1109/TNS.2006.873957
Issue Date	2006-04
Doc URL	https://hdl.handle.net/2115/13693
Type	journal article
File Information	01621344.pdf

Hokkaido University Collection of Scholarly and Academic Papers : HUSCAP

Time Domain Wake Field Computation With Boundary Element Method

Kazuhiro Fujita, Hideki Kawaguchi, Igor Zagorodnov, and Thomas Weiland

***Abstract*—We describe and demonstrate a time-domain boundary-element method for numerical computation of wake fields. The accelerator structure is modeled with a surface mesh, and the wake field is easily split from the self fields of the source particles. The formulation for three-dimensional structures is introduced first, followed by two formulations for axisymmetric structures. We briefly describe methods for computing the wake potential in a boundary-element code. Finally, we compare the fully axisymmetric formulation with codes based on the finite integration technique (FIT). The other two formulations are demonstrated with modest examples.**

***Index Terms*—Boundary element method (BEM), electric field integral equation (EFIE), magnetic field integral equation (MFIE), wake fields, wake potentials.**

I. Introduction

CHARGED particle beams traversing in accelerators interact with the surrounding structures to generate electromagnetic fields, known as wake fields. These wake fields act back on the beams, and disturb the motion of the beam itself and the following beams. As a result of the interaction, collective beam instabilities [1] that limit the maximum beam current are caused. Therefore, a good understanding of wake fields is required in order to achieve the optimal operation of an accelerator.

A practical way of calculating wake fields in realistic structures is to use numerical methods. Wake fields can be described by the Maxwell equations, and also by Kirchhoff boundary integral equations. For the two master equations, there are corresponding numerical methods, the Finite Integration Technique (FIT) [2] and the boundary element method (BEM)[3]. FIT has been widely used in conventional studies of the wake fields. For time domain calculation of wake fields, however, FIT has some problems such as numerical gird dispersion, the staircase approximation. Up to now, several approaches [4]–[8] were proposed to solve their problems. On the other hand, there are a few works on wake field computation with BEM, e.g., a frequency domain approach by Yokoya [9], boundary integral formulation based on the Hertz vectors by Miyata [10].

In this paper we propose the Time Domain Boundary Element Method (TDBEM) as one more possibility for time domain wake field computation. The TDBEM is based on the retarded Kirchhoff's boundary integral equations of electric and magnetic fields. In these equations, the total electromagnetic fields $(\mathbf{E},\mathbf{B})$ are explicitly split into the self-fields of the beams in free space $(\mathbf{E}_{\rm self},\mathbf{B}_{\rm self})$ and the wake fields $(\mathbf{E}_{\rm wake},\mathbf{B}_{\rm wake})$:

$$\mathbf{E}=\mathbf{E}_{\rm self}+\mathbf{E}_{\rm wake},\mathbf{B}=\mathbf{B}_{\rm self}+\mathbf{B}_{\rm wake}.$$

In addition, numerical mesh is generated only on boundary surfaces. In other words, no numerical mesh exists inside the volume surrounded by the surface. This allows us to easily treat a structure with curved boundaries, and the motions of charged particle beams with curved trajectories.

II. Time Domain Boundary Element Method

The TDBEM has been actively discussed in the fields of antenna analysis. Many discussions have been done mainly for numerical instabilities [11]–[13] and computation cost of calculation and memory [14], [15]. At the first part of this section, we briefly summarize these problems.

A. Time Domain EFIE and MFIE

In the following formulation, our discussion is focused on wake field analysis. So, we shall consider a coupled problem of moving charged particles and a structure with perfectly conducting walls. When the beam self-fields $\mathbf{E}_{\rm self}$ and $\mathbf{B}_{\rm self}$ illuminate the structure, the surface current density $\mathbf{K}$ and the surface charge density σ are induced on the boundary surface S since the boundary conditions of the perfect conductor must be satisfied. The current $\mathbf{K}$ and the charge σ produce secondary electric and magnetic fields in the outer region of the structure. The electric fields $\mathbf{E}(t,\mathbf{r})$ and the magnetic fields $\mathbf{B}(t,\mathbf{r})$ are then described by the following Kirchhoff's boundary integral equations in time domain (see Appendix A or [16]):

$$\begin{aligned}\mathbf{E}(t,\mathbf{r})=\mathbf{E}_{\rm self}(t,\mathbf{r})&\\ -\frac{1}{4\pi}\int_S\Bigg(\frac{1}{|\mathbf{r}-\mathbf{r}'|}\frac{\partial}{\partial t}(\mathbf{B}(t',\mathbf{r}')\times\mathbf{n}')&\\ +\left[\frac{(\mathbf{r}-\mathbf{r}')}{|\mathbf{r}-\mathbf{r}'|^3}E_n(t',\mathbf{r}')\right.&\\ \left.+\frac{(\mathbf{r}-\mathbf{r}')}{|\mathbf{r}-\mathbf{r}'|^2}\frac{\partial}{c\partial t}E_n(t',\mathbf{r}')\right]\Bigg)\,dS'&\end{aligned}\tag{1}$$

Manuscript received August 18, 2005; revised November 2, 2005. This work was supported in part by the Japan Society for the Promotion of Science under Grant-in-Aid 13640251 for Science Research.

K. Fujita is with the Division of Quantum Science and Engineering, Graduate School of Engineering, Hokkaido University, Kita-ku, Sapporo 060-8628, Japan (e-mail: fujita@eng.hokudai.ac.jp).

H. Kawaguchi is with the Department of Electrical and Electronic Engineering, Muroran Institute of Technology, Muroran 050-8585, Japan (e-mail: kawa@mmm.muroran-it.ac.jp).

I. Zagorodonov is with DESY, D-22603 Hamburg, Germany.

T. Weiland is with Technishe Universität Darmstadt, Darmstadt 64289, Germany and also with CST GmbH, Darmstadt 64289, Germany.

Digital Object Identifier 10.1109/TNS.2006.873957

0018-9499/$20.00 © 2006 IEEE

$$\mathbf{B}(t,\mathbf{r}) = \mathbf{B}_{\text{self}}(t,\mathbf{r}) - \frac{1}{4\pi}\int_S \left[\frac{(\mathbf{r}-\mathbf{r}')}{|\mathbf{r}-\mathbf{r}'|^3}\times(\mathbf{B}_t(t',\mathbf{r}')\times\mathbf{n}') + \frac{(\mathbf{r}-\mathbf{r}')}{|\mathbf{r}-\mathbf{r}'|^2}\times\frac{\partial}{c\partial t}(\mathbf{B}_t(t',\mathbf{r}')\times\mathbf{n}')\right] dS' \quad (2)$$

where $\mathbf{r}$ is the observation point in the bounded analytical region, $\mathbf{r}'$ is the point on the boundary surface, t' is the retarded time denoted by $t' = t - |\mathbf{r}-\mathbf{r}'|/c$, $\mathbf{n}'$ is the unit normal vector on the boundary surface, and E_n denotes the normal component of the electric fields on the boundary surface S. The integrand $\mathbf{B}\times\mathbf{n}$ and E_n correspond to the induced surface current density and charge density, respectively. The current density and the charge density are related each other by the continuity equation:

$$\frac{\partial\sigma}{\partial t} + \text{div}\mathbf{K} = 0. \quad (3)$$

Note that the current and charge densities in the integrands depend on not only the position $\mathbf{r}'$ but also the retarded time t'.

Equations (1) and (2) are called as the electric field integral equation (EFIE) and the magnetic field integral equation (MFIE), respectively. The first terms are the retarded fields for continuous charge distributions or the Lienard-Wiechert fields for point charges. The second terms can be interpreted as wake fields excited by the electromagnetic interaction of the self-fields and the boundary surface of a structure.

B. Discretization of Time Domain EFIE and MFIE

In order to explicitly define the direction of the surface current, we introduce the locally orthogonal coordinate systems $\mathbf{l},\mathbf{m},\mathbf{n}(\mathbf{n} = \mathbf{l}\times\mathbf{m})$ on the boundary surface. In these coordinate systems we can express the surface current as follows:

$$\mathbf{K} = K_l\mathbf{l} + K_m\mathbf{m} \quad (4)$$

where K_l and K_m are the l-component and the m-component of the surface current density, respectively. In addition, for simplicity of introducing this explicit definition, we assume here that a topology of numerical model is homotopic to torus[1], as in Fig. 1. This means that the boundary shape of numerical model is deformable from torus.

As the first step of the TDBEM formulation, we transform (2) into integral equations suitable for numerical calculations. With the explicit component expression as introduced above, we obtain finally the following two boundary integral equations (this derivation is demonstrated in Appendix B):

$$\begin{aligned}\mathbf{m}\cdot\mathbf{B}(t,\mathbf{r}) &= \mathbf{m}\cdot\mathbf{B}_{\text{self}}(t,\mathbf{r}) \\ &\quad - \frac{1}{4\pi}\int_{S'} dS'\{[-(\mathbf{m}'\cdot\mathbf{R})(\mathbf{m}\cdot\mathbf{n}') \\ &\quad + (\mathbf{n}'\cdot\mathbf{R})(\mathbf{m}\cdot\mathbf{m}')]B_m(t',\mathbf{r}') \\ &\quad + [-(\mathbf{l}'\cdot\mathbf{R})(\mathbf{m}\cdot\mathbf{n}') \\ &\quad + (\mathbf{n}'\cdot\mathbf{R})(\mathbf{m}\cdot\mathbf{l}')]B_l(t',\mathbf{r}')\} \quad (5) \\ \mathbf{l}\cdot\mathbf{B}(t,\mathbf{r}) &= \mathbf{l}\cdot\mathbf{B}_{\text{self}}(t,\mathbf{r})\end{aligned}$$

[1]The formulation described below can be applied for general structures in which the model of topology is not homotopic to torus, if it is possible to explicitly define the direction of surface current on the boundary, as in (4).

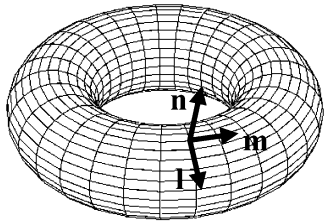

Fig. 1. Locally orthogonal coordinate defined on a torus.

$$\begin{aligned}&- \frac{1}{4\pi}\int_{S'} dS'\{[-(\mathbf{m}'\cdot\mathbf{R})(\mathbf{l}\cdot\mathbf{n}') \\ &+ (\mathbf{n}'\cdot\mathbf{R})(\mathbf{l}\cdot\mathbf{m}')]B_m.(t',\mathbf{r}') \\ &+ [-(\mathbf{l}'\cdot\mathbf{R})(\mathbf{l}\cdot\mathbf{n}') \\ &+ (\mathbf{n}'\cdot\mathbf{R})(\mathbf{l}\cdot\mathbf{l}')]B_l(t',\mathbf{r}')\} \quad (6)\end{aligned}$$

where

$$\mathbf{R} = \frac{(\mathbf{r}-\mathbf{r}')}{|\mathbf{r}-\mathbf{r}'|^3} + \frac{(\mathbf{r}-\mathbf{r}')}{|\mathbf{r}-\mathbf{r}'|^2}\frac{\partial}{c\partial t}. \quad (7)$$

B_m and B_l are the tangential components of magnetic fields corresponding to unit vectors $\mathbf{m}'$ and $\mathbf{l}'$ defined on the boundary surface, respectively. A set of the boundary integral equations (5) and (6) is discretized with the following numerical procedure: A structure with the boundary surface S is discretized by planar quadrilateral facets and the time axis is divided into constant segments Δt. The surface currents located on the boundary elements are linearly interpolated spatially and temporally. The time derivative is approximated by backward finite difference. As a result of this procedure, we can transform (5) and (6) into the following matrix equation:

$$[M_0][B_n] = [B_{\text{self}}] - \sum_{l=1}^{L}[M_l][B_{n-l}] \quad (8)$$

where $[B_l]$ denotes an unknown vector which consists of tangential components of magnetic fields on the boundary elements at time $t = l\Delta t(l = 0,\ldots,L)$, $[M_l]$ denotes a coefficient matrix determined by the boundary integral of (7) and (8) on S, L is the total number of the matrices, $[B_{\text{self}}]$ is a given vector calculated from the inner products of the tangential unit vectors and the self-fields. Fig. 2 gives an overview of the matrix equation (8). By solving (8) at each time step, the surface current density and charge induced on the boundary surface of an accelerator structure can be obtained iteratively.

Once the boundary values over all time steps are calculated, the wake fields at any position in the bounded domain can be obtained from (1) and (2).

The numerical stability of the time domain scheme (8) depends on the relation between $c\Delta t$ and the minimum facet size $h_{\min}$ or the maximum facet size $h_{\max}$. The matrix $[M_0]$ is a diagonal for $c\Delta t < h_{\min}$, and therefore inversion of the matrix is very easy. This is usually called explicit scheme, which is often unstable. On the other hand, the matrix $[M_0]$ is nondiagonal for $c\Delta t > h_{\max}$, and then inversion of $[M_0]$ becomes a complicated procedure such as the LU decomposition. This scheme is called implicit scheme, which tends to be more stable than the explicit scheme [13].

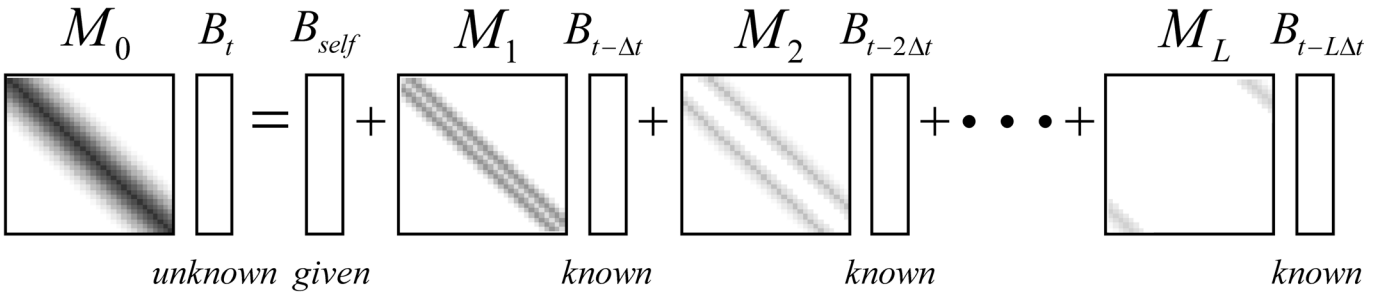

Fig. 2. Structure of the matrix equation with many matrix-vector multiplications.

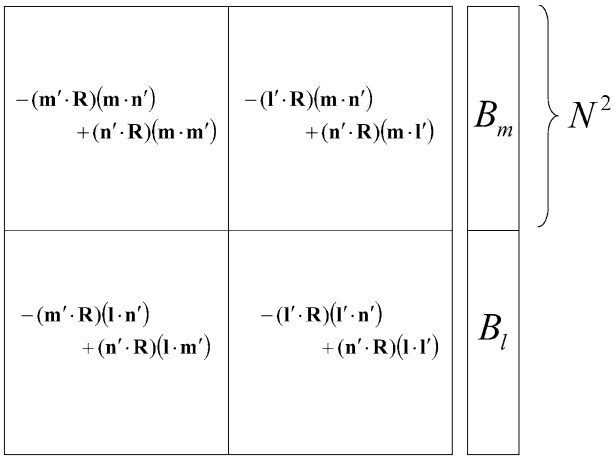

Fig. 3. Internal structure of a matrix-vector multiplication.

We adopt the implicit scheme for stably simulating wake fields in time domain, although it is costlier than the explicit scheme. In the iteration procedure of (8) using the implicit scheme, only at the first time step the LU decomposition is required, and after the second time step only the backward and the forward substitution procedures are executed for the matrix inversion, since the matrix $[M_0]$ do not depend on time.

C. Fully 3-D Simulation Scheme

The straightforward use of the matrix equation (8) for fully three-dimensional wake fields has a difficulty of large required memory. Note that one of the matrix-vector multiplications $[M_l]\,[B_{n-l}]$ in (8) has a structure as shown in Fig. 3, we can estimate the required memory for (8) as follows: if N is the number of discretization in one dimension, L is the total number of the matrices, and thus the total memory size is $8 \times 4N^4 \times L$ Byte in double precision float calculation. As an example, the required memory size reaches about 10 T Byte for $N = 200, L = 200$.

However, due to the retarded time in the time domain MFIE, a range of surface integrals are limited in striped shape area with the width $c\Delta t$. Thus, the coefficient matrices become very sparse, as shown in Fig. 2. This fact enables us to reduce the required memory size. Storing only nonzero components of the matrices, we can compress the matrices as in Fig. 4. The memory size then becomes about 380 GB for the above example $N = L = 200$.

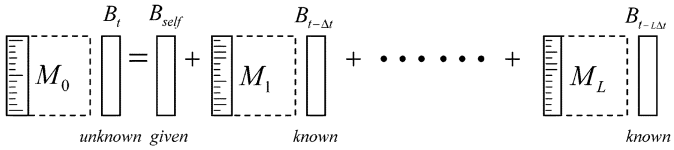

Fig. 4. Sparseness-based compression of the matrices.

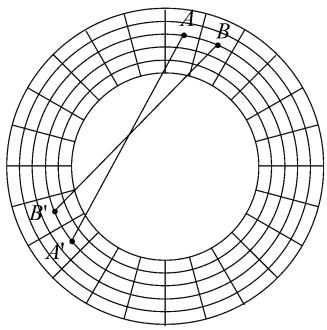

Fig. 5. Relation between two boundary element pairs AA' and BB' with the same matrix element.

D. Axis-Symmetric 2-D Simulation Scheme

In many practical cases, accelerator structures often have axis-symmetry. In this section we consider axis-symmetric wake fields.

Under the assumption of axis-symmetric fields, (1) and (2) are simplified to

$$\mathbf{E}(t,\mathbf{r}) = \mathbf{E}_{\rm ext}(t,\mathbf{r}) - \frac{1}{4\pi}\int_{S'}\left(\frac{1}{|\mathbf{r}-\mathbf{r}'|}B_m(t',\mathbf{r}')\mathbf{l}' + \left[\frac{(\mathbf{r}-\mathbf{r}')}{|\mathbf{r}-\mathbf{r}'|^3} + \frac{(\mathbf{r}-\mathbf{r}')}{|\mathbf{r}-\mathbf{r}'|^2}\frac{\partial}{c\partial t}\right]E_n(t',\mathbf{r}')\right)dS' \tag{9}$$

$$\mathbf{B}(t,\mathbf{r}) = \mathbf{B}_{\rm ext}(t,\mathbf{r}) - \frac{1}{4\pi}\int_{S'}\left(-\left[\frac{\mathbf{m}'\cdot(\mathbf{r}-\mathbf{r}')}{|\mathbf{r}-\mathbf{r}'|^3} + \frac{\mathbf{m}'\cdot(\mathbf{r}-\mathbf{r}')}{|\mathbf{r}-\mathbf{r}'|^2}\frac{\partial}{c\partial t}\right]\mathbf{n}' + \left[\frac{\mathbf{n}'\cdot(\mathbf{r}-\mathbf{r}')}{|\mathbf{r}-\mathbf{r}'|^3} + \frac{\mathbf{n}'\cdot(\mathbf{r}-\mathbf{r}')}{|\mathbf{r}-\mathbf{r}'|^2}\frac{\partial}{c\partial t}\right]\mathbf{m}'\right) \times B_m(t',\mathbf{r}')\,dS'. \tag{10}$$

Then, the induced surface current has no azimuthal components, so the total number of the unknown values is considerably decreased. For the same example $N = L = 200$, the required

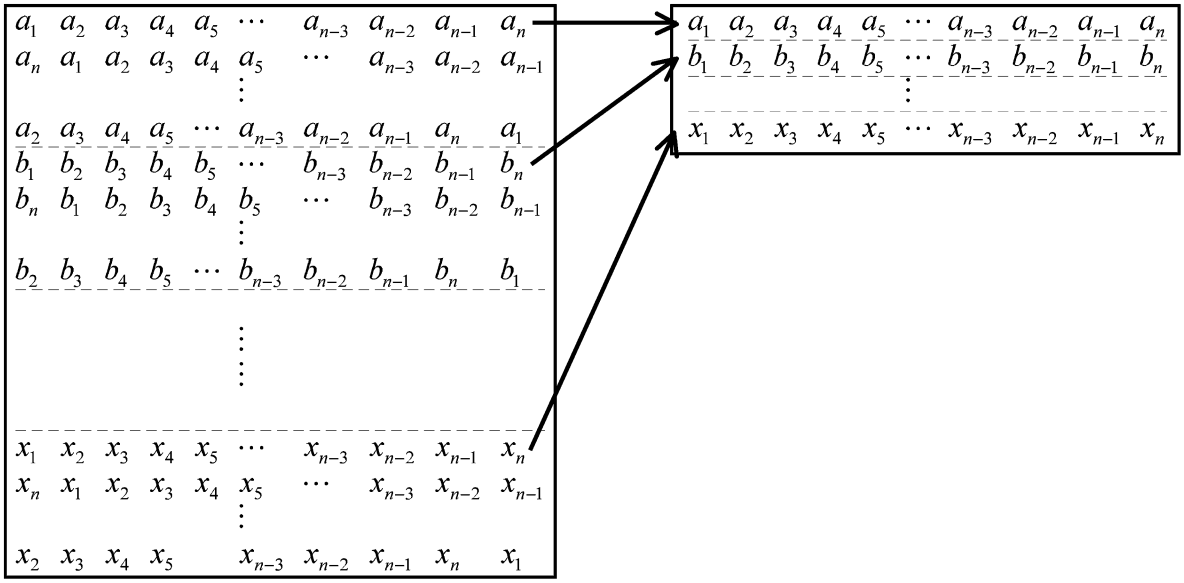

Fig. 6. Matrix compression procedure using the cyclic symmetry of matrix elements.

memory size of this formulation is 64 MB, which is a reasonable size even in a standard PC.

E. 2.5-Dimensional Simulation Scheme

When a beam moves on a trajectory with an offset to the axis in a structure with axis-symmetry, the boundary values (the surface current and charge densities) no longer have axis-symmetry. Unlike the fully 3-D simulation scheme, for this case the element array of each matrix included in (8) has cyclic patterns [17], [18].

To show this we shall consider the relation between relative position of a pair of boundary elements and matrix element allocations (Fig. 5). A boundary integral of (2) with respect of a pair of elements A and A' is same value as one of B and B', because the boundary integrals depend only on the distance $|\mathbf{r}-\mathbf{r}'|$ and the inner products between the vector $(\mathbf{r}-\mathbf{r}')$ and local unit vectors $\mathbf{l}, \mathbf{m}, \mathbf{n}$. Therefore, a matrix array pattern has cyclic symmetry as in Fig. 6, and thus we need to store only the first row among boundary elements with same radius.

By taking into account this cyclic symmetry and the sparseness of Fig. 4, all the matrices can be effectively compressed as shown in Fig. 7. We shall call this scheme as 2.5-D simulation scheme. In fact, the total memory size of a matrix equation using this scheme is 1.9 GB for $N = L = 200$, which can be treated in super computers.

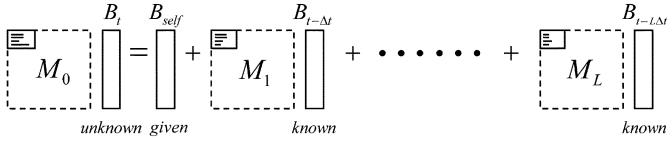

Fig. 7. Matrix equation compressed using both the sparseness and the cyclic symmetry of the TDBEM matrices in 2.5-D simulations.

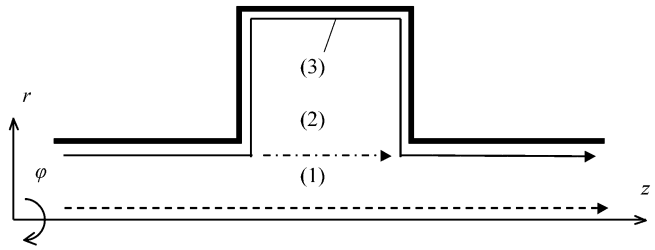

Fig. 8. Contours for wake potential calculation on the TDBEM. (1) direct integration, (2) Weiland's indirect integration, (3) the boundary surface contour (Napoly's indirect integration).

III. Wake Potential Calculation in the TDBEM

The wake potential [19] is one of important values for estimating the collective beam effects due to the wake fields. The wake potential calculation in the framework of the TDBEM is presented in this section.

The wake potentials are defined as an integral over the wake field force along a secondly test particle e following the first particle q traversing an accelerator structure with the same velocity $\mathbf{v}$ and the transversal coordinates $\mathbf{r}$ parallel to the z-axis, at a distance s behind q:

$$\mathbf{W}(\mathbf{r},s)=\frac{1}{q}\int_{-\infty}^{\infty}[\mathbf{E}_{\mathrm{wake}}(\mathbf{r},z,t)+\mathbf{v}\times\mathbf{B}_{\mathrm{wake}}(\mathbf{r},z,t)]_{t=(s+z)/c}\,dz. \quad (11)$$

For fully three-dimensional structures, we will use the direct integration according to this definition. The wake fields ($\mathbf{E}_{\mathrm{wake}}$ and $\mathbf{B}_{\mathrm{wake}}$) to be integrated in (11) can be then obtained from the boundary integral terms of (1) and (2).

For axis-symmetric structures, the infinite integration range in (11) can be transformed into a finite range with the Napoly's indirect integration method [20]. Especially, selecting the integration path along the boundary surface of a structure as shown in Fig. 8, one can calculate the wake potentials from electric and magnetic fields (B_l, B_m, and E_n) on the boundary surface, i.e., directly from the boundary values calculated with (8). Thus, for

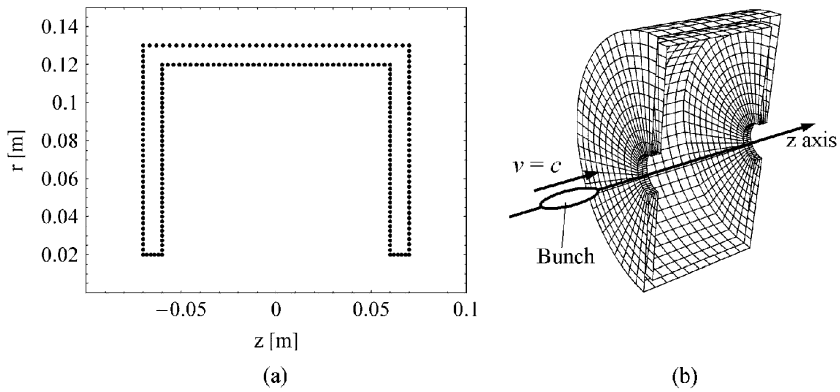

Fig. 9. Numerical model of a pillbox cavity with axisymmetry: (a) the cross-section, (b) a Gaussian bunch passing with light velocity on the symmetry axis (z axis). The total number of boundary elements along the cross-section is 250.

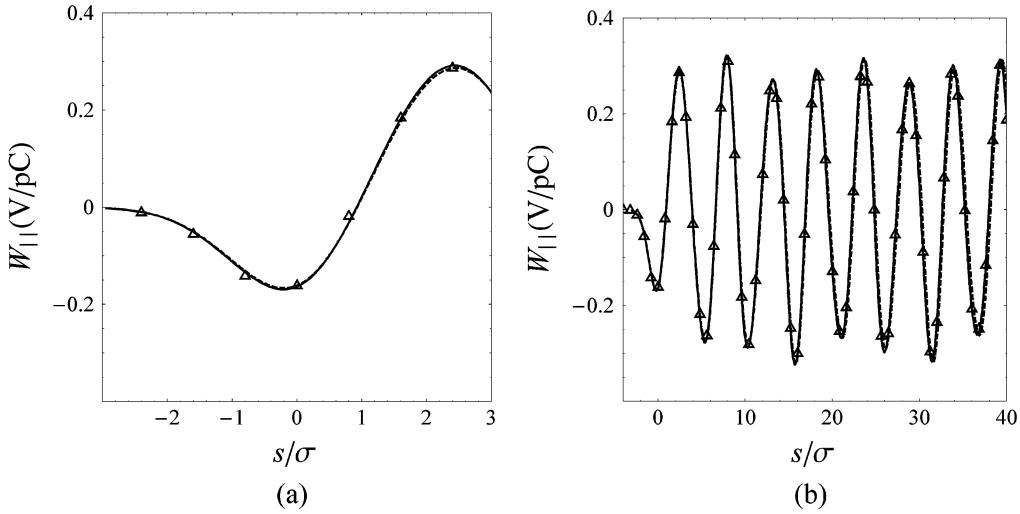

Fig. 10. Longitudinal wake potentials of the pillbox cavity for (a) short range and (b) long range (solid line: TDBEM, dashed line: FIT, triangle: analytical approach).

this case it is not necessary to calculate the fields inside the structure. On the other hand, we can also use an indirect integration path across the region inside the structure, e.g., a straight path over a gap of the structure along the beam tubes [21], as shown in Fig. 8. For such integration paths, an additional computation of the inside fields is required in the TDBEM, and numerical calculation of the wake potentials will suffer from degradation of accuracy of the fields due to the singularity of the boundary integral equations in the vicinity of the boundary.

IV. Numerical Results

In order to check numerical results of the TDBEM, we show several numerical examples for axisymmetric 2-D structures, fully 3-D one, and 2.5-D simulations.

A. Axisymmetric 2-D Simulation

1) Pillbox Cavity: Fig. 9 shows a numerical model of a pillbox cavity (gap length $g = 12$ cm, cavity radius $R = 10$ cm, tube radius $r = 2$ cm, wall depth $d = 1$ cm) and the cross-section. Short-range (a) and long-range (b) longitudinal wake potentials of a Gaussian bunch (r. m. s length $\sigma = 6$ cm, charge $Q = 1$ pC) moving with light velocity c on the z-axis (symmetry axis of rotation) are shown in Fig. 10. We can find good agreements of the TDBEM with FIT and analytical approach [22] for short and long range wake potentials.

Fig. 11 shows time signals of electric and magnetic fields (E_r, E_z, B_ϕ) calculated at two reference points inside the cavity. Good agreement between TDBEM and FIT is confirmed in the field values inside the cavity, too.

2) TESLA Cavity: To show numerical simulations of a structure with curved surfaces, a single cell of the TESLA cavity [23] (Fig. 12) is treated here. Longitudinal wake potentials of a Gaussian bunch with $\sigma = 6$ mm and $Q = 1$ nC moving with light velocity c on the axis for several different mesh sizes are shown in Fig. 13. The TDBEM simulation results are compared with those of the code ECHO, which is based on FIT. We can see that the TDBEM results converge to the ECHO result as mesh resolution σ/h (h is the maximum mesh size) is increased.

In Fig. 14, good agreements between the TDBEM and the ECHO results in long-range wake potentials for the two different σ of 3 mm and 6 mm are demonstrated.

In these simulations we use the parallelization scheme introduced in [24].

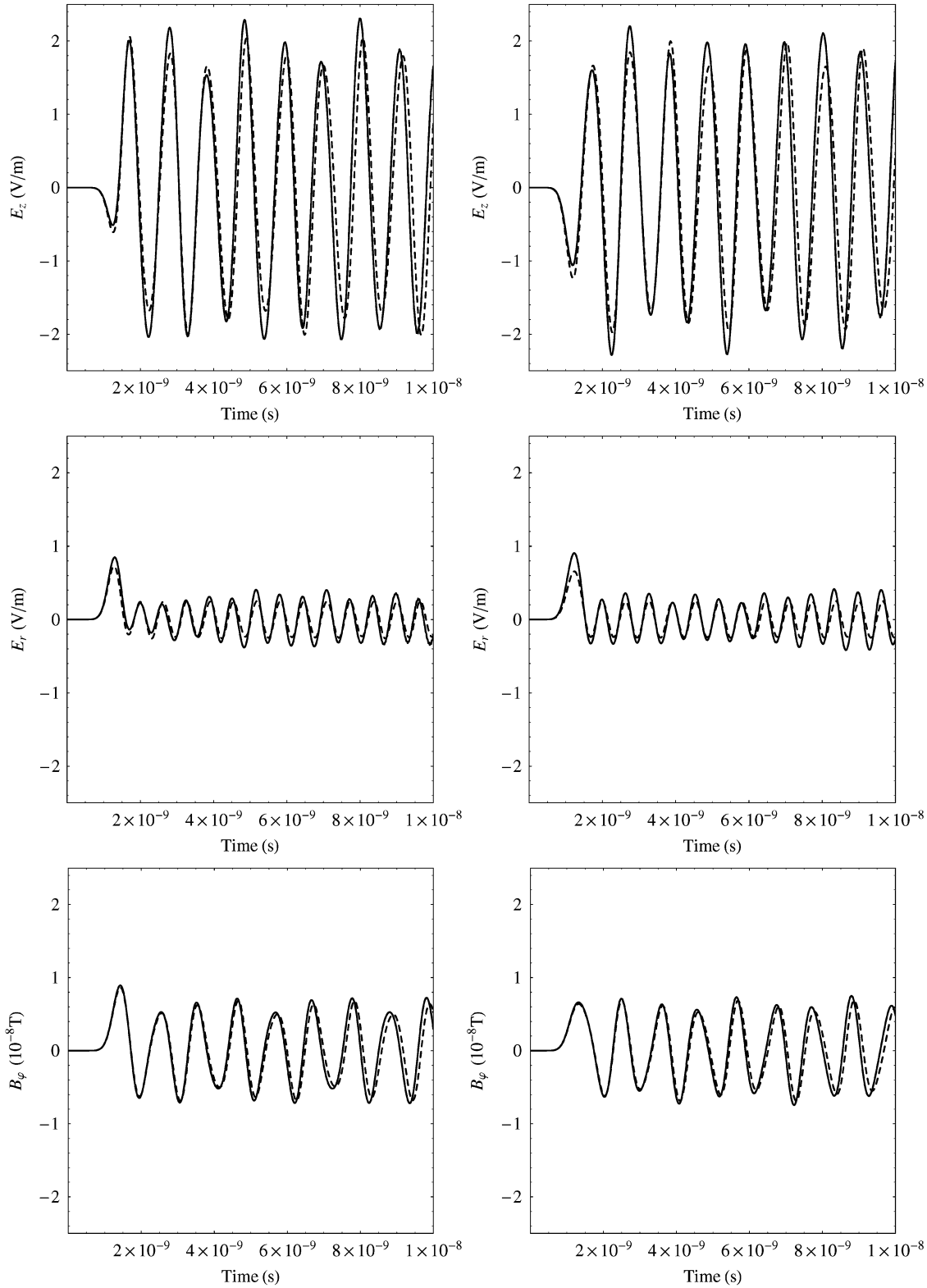

Fig. 11. Time signals of electric and magnetic fields at two reference points $(\mathrm{z},\mathrm{r}) = (0.03, 0.06)$: left, and $(-0.03, 0.06)$: right (solid line: TDBEM, dashed line FIT).

B. 2.5-D and Fully 3-D Simulation

Even if parallel computing environments are available, it is difficult to perform fully 3-D simulations and 2.5-D ones for complicated structures because very large storage memory and long CPU time are required for their simulations. We therefore use a simple model of a disc-type axisymmetric structure (inner radius $r = 4$ mm, outer radius $R = 11$ mm, wall depth $d = 2$ mm) for the verification of their schemes. To obtain the wake potentials in this case, the direct infinite integration must be used

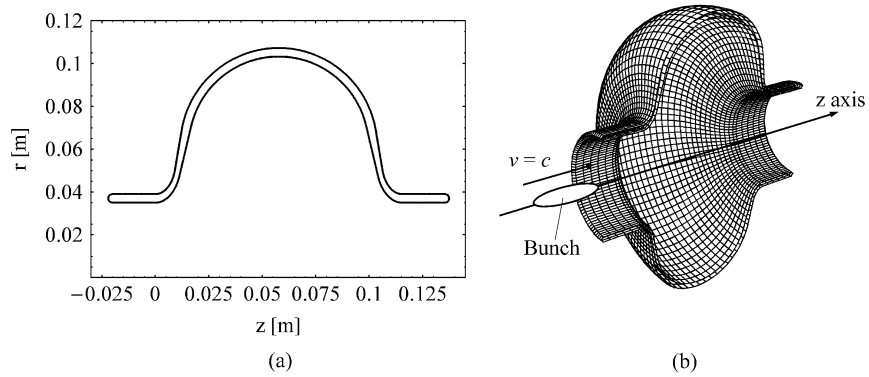

Fig. 12. Numerical model of a single cell of the TESLA cavity: (a) the cross-section, (b) a Gaussian bunch passing with light velocity on the symmetry axis (z axis). The total number of boundary elements along the cross-section is 1900.

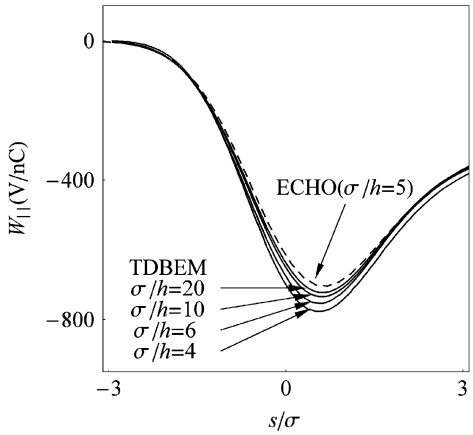

Fig. 13. Convergence of the TDBEM in wake potentials of the TESLA cavity.

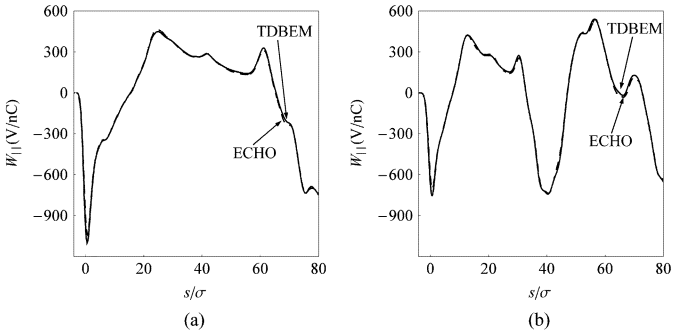

Fig. 14. Longitudinal wake potentials of the TESLA cavity for a Gaussian bunch with $\sigma =$ (a) 3 mm and (b) 6 mm (solid line: TDBEM, dashed line: ECHO).

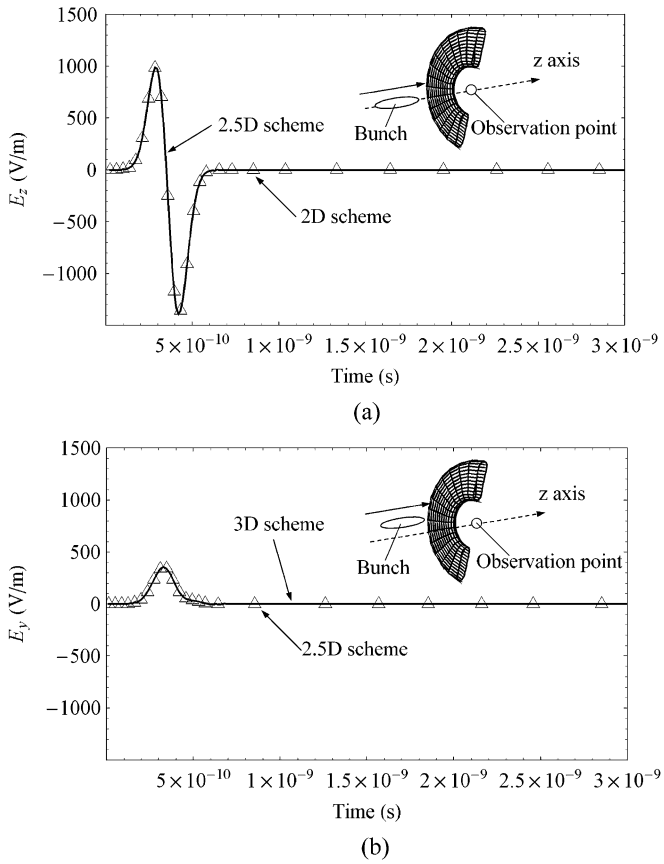

Fig. 15. Time signal of electric wake fields at the center of the disc-type structure. (a) The results of the longitudinal field E_z calculated with axisymmetric 2-D and 2.5-D schemes for a bunch moving on the z-axis. (b) The results of a transverse field E_y calculated with 2.5-D and 3-D schemes for a bunch moving with a 1.5 mm offset to the z-axis. The total number of the boundary element is 784.

because the numerical model is open structures. It seems that the number of total time step required for the fully convergent integration results become very large. So we treat wake fields themselves.

Fig. 15(a) shows axisymmetric 2-D and 2.5-D simulation results of time signals of the z-component of electric wake fields at the center of the disc. It is assumed here that the wake fields are excited by a Gaussian bunch with $\sigma = 2$ cm moving along the z-axis. The 2.5-D simulation result is consistent with the axisymmetric 2-D simulation one.

Fig. 15(b) shows 2.5-D and 3-D simulation results for the bunch moving with an offset of 1.5 mm to the z-axis. In this case, although the induced fields are three-dimensional, the numerical model is axially symmetric structures, and therefore we can apply the 2.5-D simulation scheme to this model. In this case, we compare the time signals of a transverse field E_y calculated by their schemes. We can confirm that the 3-D simulation result is consistent with the 2.5-D simulation one.

V. Conclusion

The TDBEM schemes for wake field analysis of fully 3-D and axisymmetric structures have been presented in this paper. In addition, a way to use the Napoly's indirect integration of wake potential calculation in the framework of the TDBEM has been discussed. In order to verify TDBEM-based wake field calculations, the axisymmetric 2-D scheme has been checked by numerical simulations for typical cavities, and compared with mode analysis and FIT. Moreover, the convergence of the axisymmetric 2-D scheme has been also checked in the short-range wake potential, and then it has been confirmed that TDBEM is free from numerical dispersion. In addition to the axisymmetric 2-D scheme, the 2–5D and 3-D schemes have been checked for modest examples. These schemes have advantages in wake field computations: simple modeling of curved surfaces using a surface mesh, no numerical dispersion error due to no mesh inside regions, and easy treatment of the motion of charged particle beams.

As near future works, consideration of the Napoly's indirect integration for the transverse wake potentials, and a treatment of a finite conductivity of the structure wall are still remaining. Especially TDBEM formulations of resistive material region are now under consideration, and the formulation will be changed to a composite region of vacuum and resistive material, or hybrid formulation of TDBEM and FIT, etc.

Moreover, as another future work, there are applications of the 2.5-D and 3-D schemes to wake fields on the bunch moving with curved trajectories, including shielding or cutoff by perfectly conducting structures with arbitrary shapes, such as in coherent synchrotron radiation shielded by bunch compressors or drift tubes.

Appendix A

Electromagnetic fields in vacuum can be determined from a vector potential $\mathbf{A}$ and a scalar potential ψ:

$$\mathbf{E} = -\nabla\psi - \frac{\partial \mathbf{A}}{\partial t} \tag{A1}$$

$$\mathbf{B} = \nabla \times \mathbf{A}. \tag{A2}$$

When we are interested in charged particle beams moving in a vacuum region V surrounded by perfect conductors, the electromagnetic fields on the surface S must satisfy the boundary conditions.

$$\mathbf{E} \times \mathbf{n} = 0 \tag{A3}$$

$$\mathbf{B} \cdot \mathbf{n} = 0 \tag{A4}$$

On the other hand, the electromagnetic potentials satisfy the following wave equations for the vector and scalar potentials:

$$\left(\nabla^2 - \frac{1}{c^2}\frac{\partial}{\partial t}\right)\psi = -\frac{\rho}{\varepsilon_0} - \frac{\partial}{\partial t}\left(\nabla \cdot \mathbf{A} + \mu_0\varepsilon_0\frac{\partial \psi}{\partial t}\right) \tag{A5}$$

$$\left(\nabla^2 - \frac{1}{c^2}\frac{\partial}{\partial t}\right)\mathbf{A} = -\mu_0\mathbf{A} + \nabla\left(\nabla \cdot \mathbf{A} + \mu_0\varepsilon_0\frac{\partial \psi}{\partial t}\right) \tag{A6}$$

where ε_0 is the permittivity of free space, μ_0 is the permeability of free space, and light velocity $c = (\varepsilon_0\mu_0)^{-1/2}$. As shown in [16], all components of the vector potential can be taken to be zero on the surface with an appropriate gauge transformation. That is, we have

$$\mathbf{A} = 0 \text{ on the boundary.} \tag{A7}$$

Using (A1), (A3) and (A7), we can also find

$$\psi = 0 \text{ on the boundary.} \tag{A8}$$

For a time domain boundary integral equation formulation, we use the Green's theorem on the four-dimensional time-space for any scalar functions Φ and Ψ as follows:

$$\int_\Omega \left(\frac{\partial^2\Phi}{\partial x_\lambda \partial x^\lambda}\Psi - \Phi\frac{\partial^2\Psi}{\partial x_\lambda \partial x^\lambda}\right) d\Omega = \int_\Gamma \left(\frac{\partial\Phi}{\partial x^\nu}\Psi - \Phi\frac{\partial\Psi}{\partial x^\nu}\right) d\Gamma^\nu \tag{A9}$$

where Ω is four-dimension region under consideration and Γ is the closed surface of Ω, $d\Omega = cdtdxdydz = cdtdV$ is an infinitesimal four-dimensional volume, dV is its three-dimensional sub space, and $d\Gamma^\nu$ is the outer normal infinitesimal surface element vector on Γ:

$$\begin{aligned} d\Gamma^\nu &= (dxdydz, cdtdydz, cdtdzdx, cdtdxdy) \\ &\equiv (dV,\, cdtd\mathbf{S}) \end{aligned} \tag{A10}$$

where $d\mathbf{S}$ is the outer normal infinitesimal surface element vector on S. If the region V and the boundary S are unchangeable in time, we can decompose Γ as $\Gamma = S + V_{-\infty} + V_\infty$($V_{-\infty}, V_\infty$ denotes V at $t = -\infty$ and ∞, respectively). We also use the following retarded Green function G as a fundamental solution of the wave equation:

$$G(t, \mathbf{r}; t', \mathbf{r}') = \frac{1}{4\pi}\frac{\delta\left(t' - t + \frac{|\mathbf{r}-\mathbf{r}'|}{c}\right)}{|\mathbf{r} - \mathbf{r}'|} \tag{A11}$$

where δ is the Dirac's delta function. Substituting ψ and $\mathbf{A}$, and G into Φ and Ψ of (A9), respectively, we obtain finally

$$\begin{aligned} \psi(t, \mathbf{r}) = &\frac{1}{4\pi\varepsilon_0}\int_V \frac{\rho(t', \mathbf{r}')}{|\mathbf{r} - \mathbf{r}'|}\, dV' \\ &+ \frac{1}{4\pi}\int_S \frac{1}{|\mathbf{r} - \mathbf{r}'|}\frac{\partial\psi(t', \mathbf{r}')}{\partial n'}\, dS' \\ &+ \frac{\partial g}{\partial t} \end{aligned} \tag{A12}$$

$$\begin{aligned} \mathbf{A}(t, \mathbf{r}) = &\frac{\mu_0}{4\pi}\int_V \frac{\mathbf{J}(t', \mathbf{r}')}{|\mathbf{r} - \mathbf{r}'|}\, dV' \\ &+ \frac{1}{4\pi}\int_S \frac{1}{|\mathbf{r} - \mathbf{r}'|}\frac{\partial\mathbf{A}_t(t', \mathbf{r}')}{\partial n'}\, dS' \\ &- \nabla g \end{aligned} \tag{A13}$$

where the retarded time t' is defined by

$$t' = t - \frac{|\mathbf{r} - \mathbf{r}'|}{c}, \tag{A14}$$

$\mathbf{A}_t$ is the tangential components of the vector potential on the boundary, g is a function due to gauge transformation, and $\partial/\partial n$ denotes the outer normal derivative on S. Note that the third terms with respect to g vanish in the calculation of $\mathbf{E}$ and $\mathbf{B}$ by (A1) and (A2). Then, the second terms of (A12) and (A13) are directly related to the surface charge density σ and the surface current density $\mathbf{K}$ on the perfect conductor boundary as follows:

$$\mathbf{E}\cdot\mathbf{n} = E_n = -\frac{\partial\psi}{\partial n} = -\frac{\sigma}{\varepsilon_0} \tag{A15}$$

$$\mathbf{B}\times\mathbf{n} = \frac{\partial\mathbf{A}_t}{\partial n} = -\mu_0\mathbf{K} \tag{A16}$$

where σ and $\mathbf{K}$ satisfy

$$\frac{\partial\sigma}{\partial t} + \mathrm{div}\mathbf{K} = 0. \tag{A17}$$

By substituting (A12) and (A13) into (A1) and (A2), we can obtain the following Kirchhoff's integral equations:

$$\mathbf{E}(t,\mathbf{r}) = \mathbf{E}_{\mathrm{self}}(t,\mathbf{r}) - \frac{1}{4\pi}\int_S \left(\frac{1}{|\mathbf{r}-\mathbf{r}'|}\frac{\partial}{\partial t}\left(\frac{\partial\mathbf{A}_t(t',\mathbf{r}')}{\partial n'}\right) - \left[\frac{(\mathbf{r}-\mathbf{r}')}{|\mathbf{r}-\mathbf{r}'|^3} + \frac{(\mathbf{r}-\mathbf{r}')}{|\mathbf{r}-\mathbf{r}'|^2}\frac{\partial}{c\partial t}\right]\frac{\partial\psi(t',\mathbf{r}')}{\partial n'}\right)\mathrm{dS}' \tag{A18}$$

$$\mathbf{B}(t,\mathbf{r}) = \mathbf{B}_{\mathrm{self}}(t,\mathbf{r}) - \frac{1}{4\pi}\int_S \left[\frac{(\mathbf{r}-\mathbf{r}')}{|\mathbf{r}-\mathbf{r}'|^3} + \frac{(\mathbf{r}-\mathbf{r}')}{|\mathbf{r}-\mathbf{r}'|^2}\frac{\partial}{c\partial t}\right] \times \frac{\partial\mathbf{A}_t(t',\mathbf{r}')}{\partial n'}\,dS'. \tag{A19}$$

Therefore, (1) and (2) can be obtained from (A18) and (A19) using (A15) and (A16).

APPENDIX B

In the locally orthogonal coordinate systems $\mathbf{l},\mathbf{m},\mathbf{n}(\mathbf{n}=\mathbf{l}\times\mathbf{m})$ as in Fig. 1, magnetic fields $\mathbf{B}$ and the vector $\mathbf{R}$ in (7) can be decomposed into their components as follows:

$$\mathbf{B} = (\mathbf{B}\cdot\mathbf{l})\mathbf{l} + (\mathbf{B}\cdot\mathbf{m})\mathbf{m} + (\mathbf{B}\cdot\mathbf{n})\mathbf{n} \tag{A20}$$

$$\mathbf{R} = (\mathbf{R}\cdot\mathbf{l})\mathbf{l} + (\mathbf{R}\cdot\mathbf{m})\mathbf{m} + (\mathbf{R}\cdot\mathbf{n})\mathbf{n}. \tag{A21}$$

Combining (A16) and (A20), we find

$$\mathbf{B}\times\mathbf{n} = B_m\mathbf{l} - B_l\mathbf{m} \tag{A22}$$

where $B_l \equiv \mathbf{B}\cdot\mathbf{l}$ and $B_m \equiv \mathbf{B}\cdot\mathbf{m}$. By substituting (A21) and (A22) into (2), we have

$$\mathbf{B}(t,\mathbf{r}) = \mathbf{B}_{\mathrm{self}}(t,\mathbf{r}) - \frac{1}{4\pi}\int_{S'} dS'\{[-(\mathbf{m}'\cdot\mathbf{R})\mathbf{n}' + (\mathbf{n}'\cdot\mathbf{R})\mathbf{m}'] \times B_m(t',\mathbf{r}') + [-(\mathbf{l}'\cdot\mathbf{R})\mathbf{n}' + (\mathbf{n}'\cdot\mathbf{R})\mathbf{l}']B_l(t',\mathbf{r}')\}. \tag{A23}$$

Finally, taking the inner products of (A23) with the tangential vectors $\mathbf{l},\mathbf{m}$, respectively, we obtain (5) and (6).

REFERENCES

[1] W. C. Chao, *Physics of Collective Beam Instabilities in High Energy Accelerators*. New York: Wiley, 1993.

[2] T. Weiland, "Time domain electromagnetic field computation with finite difference methods," in *Int. J. Numer. Modeling: Electron. Networks*, vol. 9, 1996, pp. 295–319.

[3] C. A. Brebbia, *The Boundary Element Method for Engineers*. London, U.K.: Pentech, 1978.

[4] K. R. Umashankar, A. Taflove, and B. Beker, "Calculation and experimental validation of induced currents on coupled wires in an arbitrary shaped cavity," *IEEE Trans. Antennas Propag.*, vol. 35, no. 11, pp. 1248–1257, Nov. 1987.

[5] T. G. Jugens and F. A. Harfoush, "Finite difference time domain modeling of particle accelerators," in *Proc. PAC*, Chicago, IL, 1989, pp. 866–868.

[6] M. Dehler, "Numerical wake calculations using an equivalence principle," *Particle Accelerators*, vol. 49, pp. 105–116, 1995.

[7] I. Zagorodnov, R. Schuhmann, and T. Weiland, "Long-time numerical computation of electromagnetic fields in the vicinity of a relativistic source," *J. Comput. Phys.*, vol. 191, pp. 525–541, 2003.

[8] R. Hampel, I. Zagorodnov, and T. Weiland, "New discritization scheme for wake field computation in cylindrically symmetric structures," in *Proc. EPAC*, Lucerne, Switzerland, 2004, pp. 2559–2561.

[9] K. Yokoya, "Resistive wall impedance of beam pipes of general cross section," *Particle Accelerators*, vol. 41, pp. 221–248, 1993.

[10] K. Miyata, "Three-dimensional wake field analysis by boundary element method," in *Proc. PAC*, Washington, D.C., 1987, pp. 1340–1342.

[11] B. P. Rynne, "Stability and convergence of time marching methods in scattering problems," *J. Appl. Mathematics*, vol. 35, pp. 297–310, 1985.

[12] P. J. Davies, "Stability of time-marching numerical schemes for the electric field integral equation," *J. Electr. Waves Applicat.*, vol. 8, no. 1, pp. 85–114, 1994.

[13] H. Kawaguchi and T. Homma, "Consideration on numerical instability of Dirichlet Gauge BEM," *IEEE Trans. Magn.*, vol. 32, no. 3, pp. 914–917, May 1996.

[14] S. P. Walker and C. Y. Leung, "Parallel computation of time-domain integral equation analyzes of electromagnetic scattering and RCS," *IEEE Trans. Antennas Propag.*, vol. 45, no. 4, pp. 614–619, Apr. 1997.

[15] S. J. Dodson, S. P. Walker, and M. J. Bluck, "Costs and cost scaling in time-domain integral equation analysis of electromagnetic scattering," *IEEE Antennas Propag. Mag.*, vol. 40, no. 4, pp. 12–21, Aug. 1998.

[16] H. Kawaguchi, "Time-domain analysis of electromagnetic wave fields by boundary integral equation method," *Eng. Anal. Boundary Elements*, vol. 27, pp. 291–304, 2003.

[17] H. Kawaguchi, "Stable time-domain boundary integral equation method for axisymmetric coupled charge-electromagnetic field problems," *IEEE Trans. Magn.*, vol. 38, no. 2, pp. 749–752, Mar. 2002.

[18] K. Fujita and H. Kawaguchi, "2.5-dimensional simulation of electromagnetic fields with time domain boundary element method," *Trans. JASCOME, J. Boundary Element Methods*, no. 04-040 925, pp. 19–22, 2004. (in Japanese).

[19] B. W. Zotter and S. A. Kheifets, *Impedances and Wakes in High-Energy Particle Accelerators*, Singapore: World Scientific, 1998.

[20] O. Napoly, Y. Chin, and B. Zotter, "A generalized method for calculating wake potentials," *Nucl. Instrum. Methods Phys. Res. A*, vol. 344, p. 255, 1993.

[21] T. Weiland, "Comment on wake field computation in time domain," *Nucl. Instrum. Methods*, vol. 216, pp. 31–34, 1983.

[22] T. Weiland and B. Zotter, "Wake potentials of a relativistic current in a cavity," *Particle Accelerators*, vol. 11, pp. 143–151, 1981.

[23] P. Hülsmann, W. F. O. Müller, and H. Klein, "The diffraction model and its applicability for wakefield calculations," in *Proc. XX Int. Linac Conf.*, Monterey, CA, 2000, pp. 21.08–25.08.

[24] D. Poljak and H. Kawaguchi, Eds., *Time Domain Techniques in Computational Electromagnetics 4*. Southampton, U.K.: WIT Press, 2004, ch. 1, pp. 1–36.